SolarPACES 2024, 30th International Conference on Concentrating Solar Power, Thermal, and Chemical Energy Systems

Analysis and Simulation

https://doi.org/10.52825/solarpaces.v3i.2383

© Authors. This work is licensed under a Creative Commons Attribution 4.0 International License

Published: 28 Nov. 2025

# Characterisation of the Wind Convection Losses in Plain and Ribbed Tubes of Solar Central Receivers via Tube-Resolved CFD Simulations

José Martín-Martínez<sup>1,2,\*</sup> , Rafael Pérez-Álvarez<sup>1</sup>, Diego Martínez-Plaza<sup>2</sup>, and Antonio Acosta-Iborra<sup>1</sup>

<sup>1</sup>Carlos III University of Madrid, Dept. of Thermal and Fluids Engineering, 28911 Leganés, Spain <sup>2</sup>EU-Solaris ERIC, 04200 Tabernas, Spain

\*Correspondence: Jose Martin Martinez, jose.mmartinez@alumnos.uc3m.es

**Abstract.** Convective losses due to wind affect the thermal efficiency of external central receivers of solar power towers (SPT), but their full characterization is still an unresolved question. Furthermore, detailed assessment of these convective losses in new designs, such ribbed tube central receivers, is nearly inexistent. The aim of this study is (a) to parameterize the wind convection coefficient and its local distribution in all the tubes and panels of an external central receiver, and (b) to compare the wind convection coefficients in conventional plain tube receivers and in ribbed tubes receivers designed to enhance heat transfer from the tube wall to the heat transfer fluid (HTF). To gain a detailed understanding of the complex heat transfer phenomena involved, this work is entirely developed through Computational Fluid Dynamics (CFD) simulations in a three-dimensional (3D) domain that describes all the absorber tubes in the receiver. Overall results of the simulations are practically validated against experimental results available in the literature [1].

**Keywords:** CFD Simulation, Forced Convection, External Receiver, Ribbed Tubes, Corrugated Tubes, Mixed Convection, Solar Power Tower (SPT)

#### 1. Introduction

This study investigates the forced convection coefficient of a solar power tower (SPT) external receiver based on a commercial-scale plant [2]. The research focuses on two receiver configurations concerning the absorber tubes: plain tubes and ribbed tubes, with the latter being explored by other authors [3] to enhance thermal performance. Currently, the most well-known convection coefficient is the one provided in [1], which specifies only an average value of the forced convection heat transfer coefficient at the receiver level. However, [1] highlights challenges in accurately modelling forced convection, such as roughness due to welded tubes, as well as the effects of free-stream turbulence and abrupt corners in the receiver design. These unaccounted factors could cause the forced convection component to be 50-100% larger than current correlations according to [1], indicating the need for further investigation. Due to this limitation, authors often apply various shape factors to this correlation [2] to spatially distribute the forced convection coefficient, typically assuming a symmetrical distribution along the circumference of the receiver tubes. This research aims to clarify whether this symmetrical distribution is appropriate and to elucidate how the coefficient is actually distributed along the receiver. The study validates simulation models, and assess the impact of ribbing on heat

transfer efficiency, with results expected to provide insights into a distribution of forced convection heat transfer coefficients that more accurately reflects real operating conditions.

# 2. System description

The SPT receiver parameters used in the present study are based on a commercial scale power plant described in a previous work [2]. The plant is equipped with a 120MWth external receiver whose absorber tubes are oriented vertically and have a length of  $H=10.5\,\mathrm{m}$  exposed to radiation (i.e. receiver height), outer diameter of  $D=4.22\,\mathrm{cm}$ , wall thickness of  $th=1.65\,\mathrm{mm}$  and tube separation pitch of B=0.08D. The receiver consists of two circuits, each with nine panels. As indicated in Figure 1(a), only one circuit with nine panels will be studied owing to the system symmetry. Each panel is constructed from 32 tubes with the specifications outlined above. The main wind parameters relevant for this research work are the air temperature,  $T_\infty=300\,\mathrm{K}$ , and the horizontal wind velocity,  $\emph{v}=20\,\mathrm{m/s}$ , whose direction relative to the receiver is shown in Figure 1.

In this study, to reduce computational costs, a 1-metre section of the total tube length H was simulated. This length is considered enough given the horizontal direction of the wind and the resulting small variations for the air flow field in axial direction.

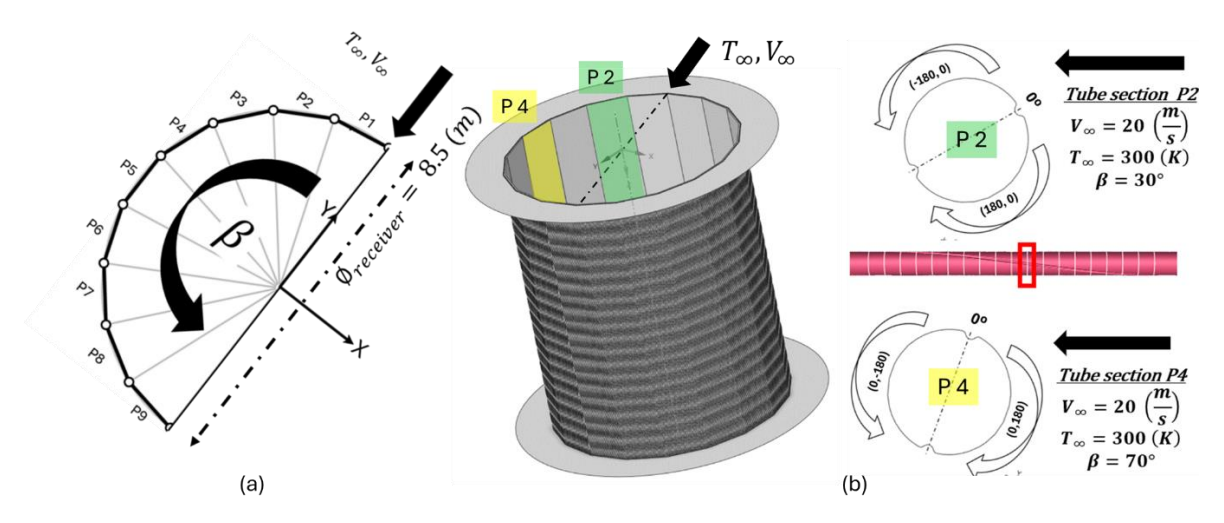


**Figure 1.** a) central receiver domain referencing system, b): panel 2 and panel 4 tube cross-sections at the middle length of the tube (in red colour).

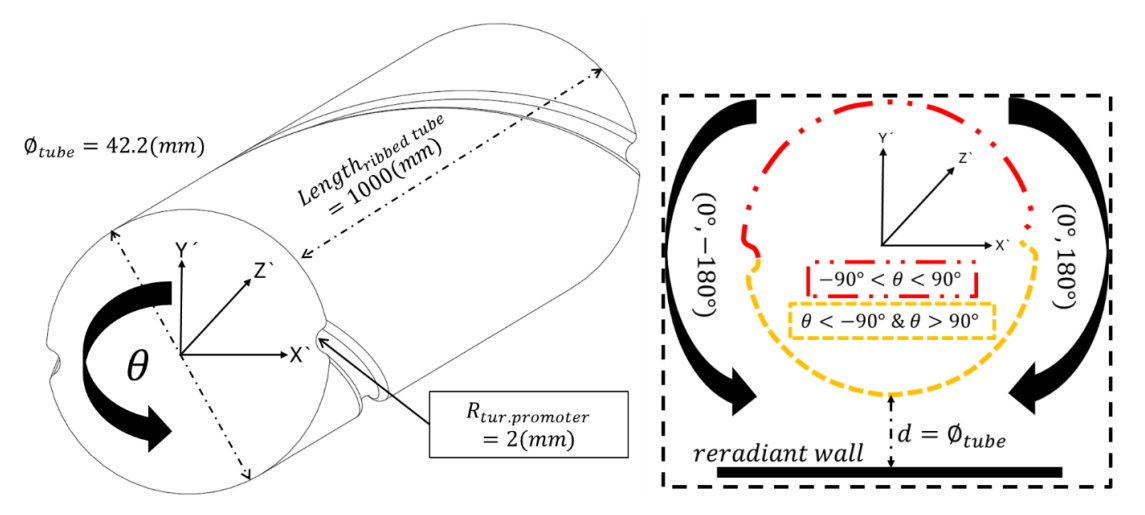


Figure 2. Tube domain referencing system and general dimensions.

The referencing system and the simulation domain used throughout this work are shown in Figures 1 and 2. They refer to the central receiver ( $\beta \& X, Y, Z$ ) and its tubes ( $\theta \& X, Y, Z$ ), respectively. The domain includes only the air outside the tubes, which is limited internally by the reradiant wall of the receiver and externally by an outer boundary separated  $15\Phi$  from the receiver, where  $\Phi$  indicates the receiver diameter.

As mentioned before, two different receiver configurations were studied: a configuration with a normal (plain) tube and a configuration with a ribbed tube. The ribbed tube has a double helix of corrugations, with each corrugation separated by 180° and having a pitch of 1 turn per meter. The corrugation has a radius of 2 mm (Figure 2). Within the domain  $Z \in [0.25 \text{ m}, 0.75 \text{ m}]$  the corrugations are positioned: a) front side  $\theta_{corrugation} = -90^{\circ}$  for Z = 0.25 (m) and  $\theta_{corrugation} = 90^{\circ}$  for Z = 0.75 (m) and b) rear side  $\theta_{corrugation} = 90^{\circ}$  for Z = 0.25 (m),  $\theta_{corrugation} = 180^{\circ}$  for Z = 0.5 (m) and  $\theta_{corrugation} = -90^{\circ}$  for Z = 0.75 (m), thus capturing a complete turn within the model for rear and front positions.

Figure 3 shows the CFD domain used to simulate wind flow around half of the receiver. It includes nine panels and extends 127.5 m in the x-direction, 25.5 m in the y-direction, and 1 m in height. Boundary conditions include uniform inlet velocity and temperature, pressure outlet, symmetry planes, and adiabatic walls with zero shear (for z=0 and z=1 m). Only the external air region is modelled.

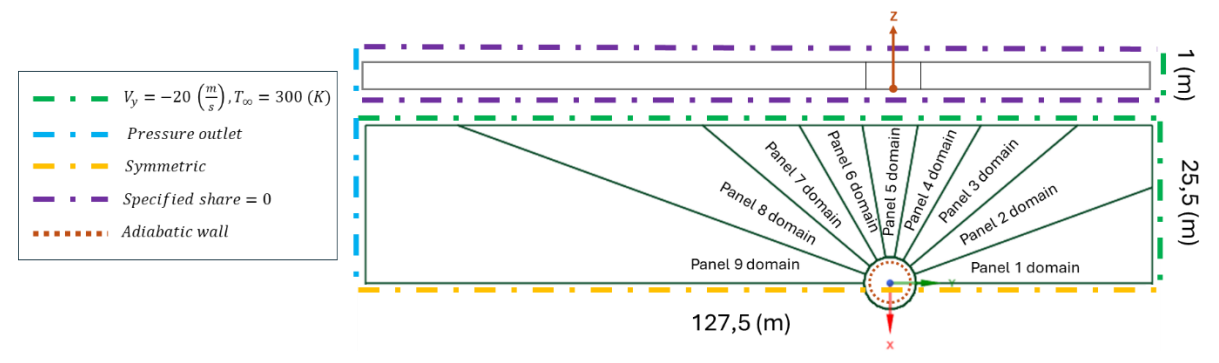


Figure 3. Boundary conditions and dimensions of the CFD simulation domain.

### 3. Methods

## 3.1 Governing Equations and convection coefficients

The governing equations considered here were the Navier-Stokes mass, momentum and energy balances for the air outside the tubes in the domain described in Section 2. Air properties, including density, were evaluated at the average boundary layer temperature as in [4] and [5]. The wind velocity direction and magnitude were imposed at the boundary where the air enters the domain, far from the tubes. Pressure exit conditions were defined where the air leaves the domain. Non-slip conditions were considered at the outer surface of the tubes and the reradiant surface. The upper and lower boundaries (Z = 0 m and Z = 1 m) were modelled using a non-reflecting, free-slip boundary condition to approximate the tube continuation. In this first study, a uniform temperature  $T_{tube\_wall} = 680~K$  was set at the exterior surface of the tube representing an average value taken from [2]. Note that the forced convection coefficient of the air is weakly influenced by the wall temperature, contrary to natural convection and radiation, which are not considered in this work.

At a given tube "i" and panel "j", the forced convection coefficient,  $h_{fc,i,j}(\theta,Z)$ , resulting from the simulations was first determined locally, i.e. at any position  $\theta$  and Z of the outer tube surface, by dividing the net heat flux at this position by the temperature difference between the tube wall and the main air flow,  $T_{\infty}$ . Then, a representative circumferential distribution of the

convection coefficient in a given panel was computed as the mean of the air convection coefficient along the entire axial length of the tube and averaged for all the tubes of a panel:

$$\bar{h}_{fc_{panel\,j}}(\theta) = \frac{1}{32} \sum_{i=1}^{32} \frac{1}{H - 2Z_{ex}} \int_{Z = Z_{ex}}^{Z = H - Z_{ex}} h_{fc,i,j}(\theta, Z) dZ \tag{1}$$

Where  $Z_{ex}=0.25\,m$  is a sufficient distance from the tube inlet and exit to avoid edge effects on  $\bar{h}_{f\,c_{panel}}(\theta)$ . Thus, the panel convection coefficient averaged along the tube perimeter is:

$$\bar{\bar{h}}_{fc_{panel}j} = \frac{1}{2\pi} \int_0^{2\pi} \bar{h}_{fc_{panel}j}(\theta) d\theta$$
 (2)

The mean value of the convection coefficient in the receiver was calculated with an average extended to all the 9 simulated panels:

$$\bar{h}_{fc_{receiver}} = \frac{\sum_{j=1}^{9} \bar{h}_{fc_{panel j}}}{9} \tag{3}$$

In order to validate the simulation results, the receiver convection coefficient  $\bar{h}_{S\&K}$  obtained from the correlation proposed by Siebers & Kraabel [1] was employed:

$$\bar{h}_{S\&K} = \left(\frac{k \cdot N u_{\Phi}}{\Phi}^{3.2} + \frac{k \cdot N u_{H}}{H}^{3.2}\right)^{1/3.2} \tag{4}$$

Where k is the air thermal conductivity,  $\Phi$  is the receiver diameter,  $Nu_H$  and  $Nu_\Phi$  are the Nusselt numbers for natural and forced convection, respectively, which are determined with the correlations proposed in [1]. Natural convection is neglected ( $Nu_H \approx 0$ ) compared to forced convection for the wind conditions studied here. Following [5], a circumferential distribution of the convection coefficient can be estimated from  $\bar{h}_{S\&K}$  using a distribution factor which depends on the circumferential angle  $\theta$ :

$$\bar{h}_{S\&K}(\theta) = (\sin(\theta) + 1)\,\bar{h}_{S\&K} \tag{5}$$

# 3.2 Computational mesh and numerical solution

The commercial CFD software ANSYS Fluent (version 2024 R1) was used to simulate the receiver models with plain and ribbed tubes described in Section 2. The Reynolds-averaged Navier-Stokes equations were solved in a three-dimensional domain with second order accuracy in the convective and diffusive terms. Turbulence was modelled using the k- ω SST equations, which are suitable to capture the effects of adverse pressure gradients around the receiver. Two simulation approaches were used: a Simultaneous Simulation (S.S.) of the complete domain, employed in the case of the plain tube configuration, and a Piecewise Simulation method (P.S.) utilized in the case of the ribbed tube configuration to reduce the computational cost. The piecewise method divided the domain into overlapping sections, each one comprising a panel and a fraction of the neighbour panels. Sections are sequentially solved in the wind direction and then backwards, iteratively transferring boundary conditions from one section to another, to address recirculation effects. In both approaches, the employed mesh configurations were poly-hexahedral, ranging from 30 to 50 million cells, maintaining the y+ parameter between 0.1 and 10. The results were obtained for steady-state formulation of the equations, restricting the unsteady formulation to only the cases where transient flow structures were observed. Results of the convective coefficient were averaged over multiple iterations or timesteps.

#### 4. Results and Discussion

#### 4.1 Initial validation

A mesh sensitivity analysis was performed by increasing the number of cells in the employed meshes. For a plain tube in the Simultaneous Simulation (S.S.), the uncertainty was  $\pm 2\%$ ; for the Piecewise Simulation (P.S.),  $\pm 6.3\%$ . A temperature analysis revealed negligible uncertainty ( $<\pm 1\%$ ). Combined configurations showed a minor uncertainty of  $\pm 1.1\%$ , while ribbed tubes under P.S. reached  $\pm 7\%$ . Data processing errors were estimated at  $\pm 5\%$ . Overall uncertainty, calculated using the Root Sum of Squares (RSS) method, is  $\pm 11\%$ .

Validation against the Siebers & Kraabel correlation [1] yielded a deviation of -30.9% (Table 1), which is within the  $\pm50\%$  range reported in [1]. Additionally, a comparison between constant wall temperature (680 K) and a non-uniform circumferential profile showed similar forced convection coefficients, validating the modelling assumption.

## 4.2 Plain tube receiver configuration

Using the definitions of the presented in Section 3.1, Figure 4 shows the circumferential distribution of the air convection coefficient for each panel,  $\bar{h}_{fc_{panel}}(\theta)$ , where panel 0 corresponds to  $\beta=0^\circ$  (a panel positioned perpendicular to the wind direction in a special case evaluated separately so check the sensitivity of the results to wind direction relative to the panel plane), panel 1 corresponds to  $\beta=10^\circ$  and panel 9 with  $\beta=170^\circ$  according to the coordinates system presented in Figures 1 and 2. Table 1 summarises the average panel convection coefficients  $\bar{h}_{fc_{panel}}$  the maximum and minimum values of the circumferential distribution,  $\bar{h}_{fc}(\theta_i)$ , and the angular location of the peak value. Panel 2 presents the highest average and peak values, while panels 4, 5, 6, and 7 show the lowest. The distributions for panels 0 and 6, along with the S&K-0 reference (Equation 5), appear circumferentially symmetric, although the location of their maxima differs. For instance, panel 6 peaks at  $\theta=0^\circ$  whereas panel 0 peaks at  $\theta=\pm77.5^\circ$ , affecting their agreement with the S&K profile. The angular position of the peak in each panel, as shown in Table 1, reflects the influence of wind orientation and local flow dynamics, which often leads to asymmetric distributions not captured by the analytical model.

**Table 1.** Forced convection coefficient  $(W/m^2K)$  CFD results and S&K obtained according to [1].

Panel	$\overline{ar{m{h}}}_{fc_{panelj}}$	$\max_{\boldsymbol{\theta}} \left( \overline{h}_{fc_{panelj}}(\boldsymbol{\theta}) \right)$	h̄ peak θ (°)	$min\Big(\overline{h}_{fc_{panelj}}(oldsymbol{ heta})\Big)$		
j = 0	43.7	66.8	±77.5	22.2		
j = 1	42.4	92.3	-43.5	12.0		
j = 2	67.3	129.9	-43.5	30.3		
j = 3	56.9	87.2	-43.5	30.5		
j = 4	19.8	37.9	-139.5	9.3		
j = 5	9.3	17.6	144.0	2.5		
j = 6	17.2	26.2	0.0	8.0		
j = 7	17.1	23.5	107.0	8.3		
j = 8	36.5	70.6	138.0	16.7		
j = 9	47.4	108.2	40.5	14.8		
h plain	34.9	N/A	N/A	N/A		
rec.						
h S&K-θ	50.5	100.9	0.0	0.0		
Deviation	-30.9%	N/A	N/A	N/A		

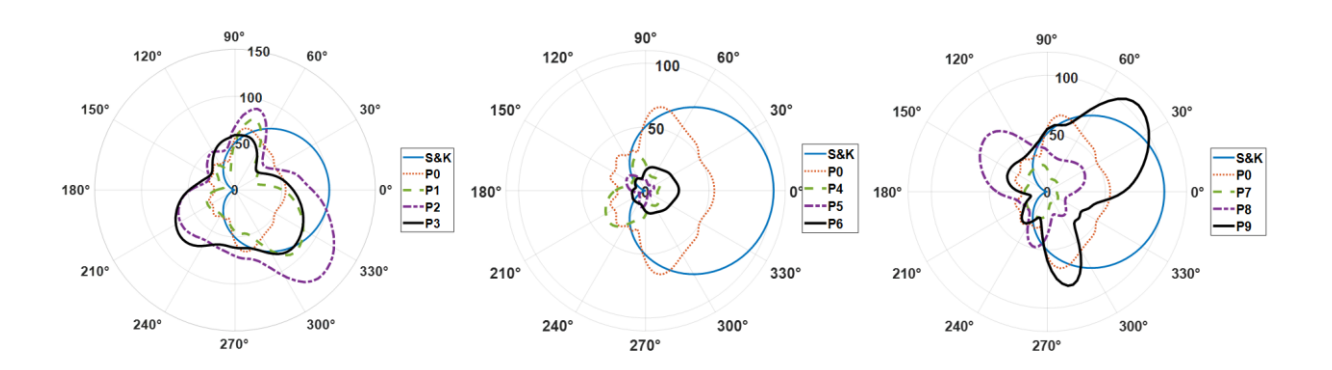
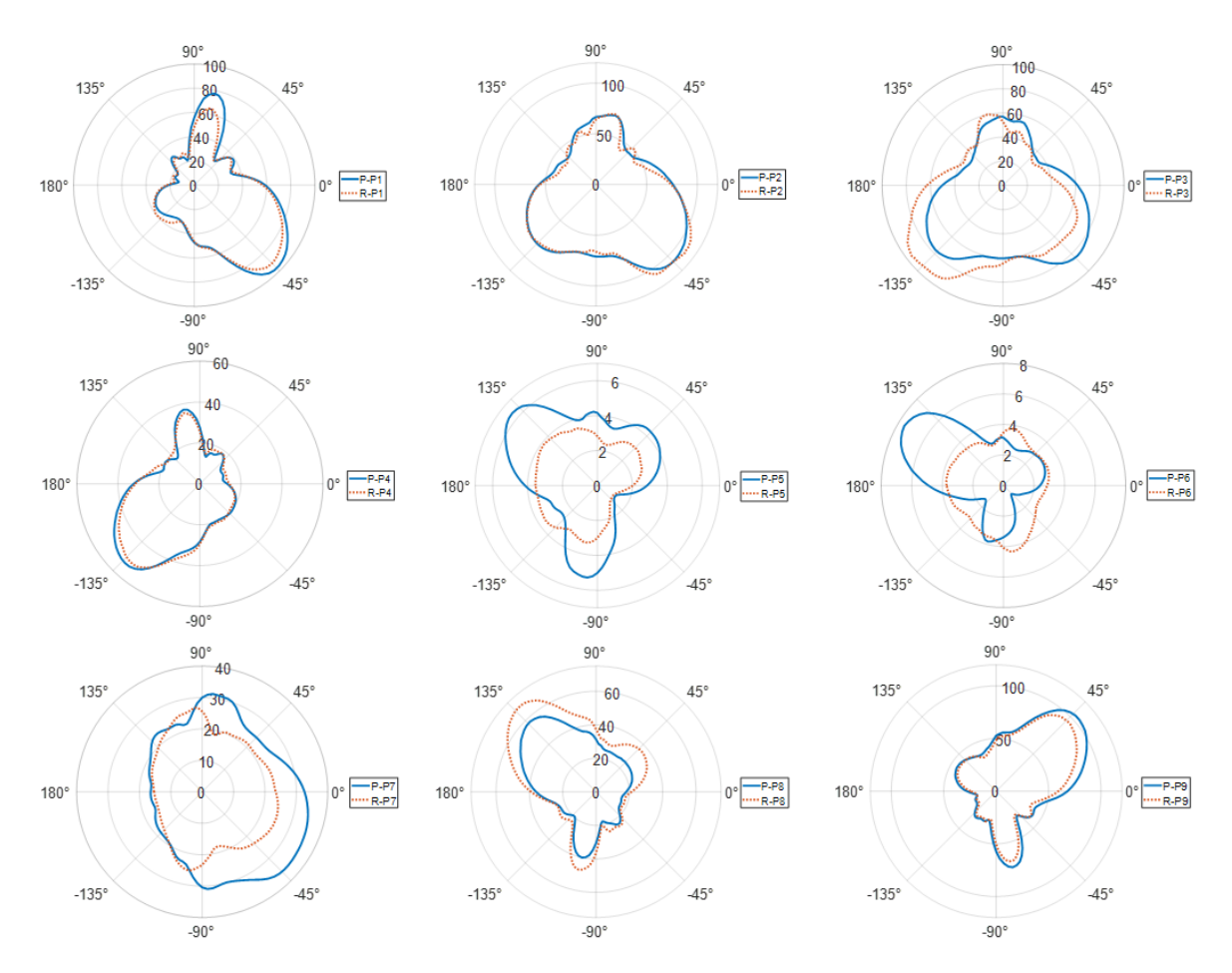


Figure 4. Forced convection coefficient plain tubes CFD results and Siebers & Kraabel correlation [1].

# 4.3 Ribbed vs plain tube receiver configurations

The simulations of the receiver with the ribbed tubes were conducted using the Piecewise Simulation method due to their high computational cost. Due to the novelty of ribbed tube receivers, there are no available correlation or experimental result of their wind convection coefficient for validation. Figure 5 displays the distribution of  $\bar{h}_{fc_{panel}j}$  (0), across various ribbed and plain tube panels, with Table 2 summarising these values for plain and ribbed configurations. The results according to Table 2, and considering that distributions for plain and ribbed tubes are similar in some of the panels, reveal that panel 2 gives the largest maximum value,  $\max_{\theta} \left( \bar{h}_{fc_{panel}j}(\theta) \right)$ , and average value,  $\bar{h}_{fc_{panel}j}$ , while panels 4, 5, 6, and 7 exhibit the lowest values, with panels 5 and 6 potentially not accurately representing the actual flow in that region. The Siebers & Kraabel correlation (Equation 4) yields a value of  $\bar{h}_{S\&K}=50.45$ , which is higher than the simulation results for  $\bar{h}_{cf_{receiver}}$ .



**Figure 5.** Forced convection coefficient distribution for plain (P) and ribbed (R) tubes receivers simulated with P.R. models.

Comparisons between Simultaneous and Piecewise Simulation methods in Table 2 show that panels 1, 2, 3, and 9 exhibit high agreement between complete and Piecewise Simulation configurations, but relative deviations are significant for panels 5 and 6, which have a minor impact due to their lower heat transfer rates. Comparisons between ribbed and plain tubes, analysed using the Piecewise Simulation method, show similar results for  $\bar{h}_{f\,c_{panel}}$ ,  $\bar{h}_{f\,c_{receiver}}$ . Aside from some local deviations, the ribbed tubes configuration does not significantly impact the average wind convection coefficients compared to those of the plain tubes.

**Table 2.** Results of forces convection coefficient  $(W/m^2K)$  for ribbed and plain tubes

$\overline{h}_{ ext{fc\_panel}}$	P1	P2	Р3	P4	P5	P6	P7	P8	P9	R. mean
Plain (S.S.)	42.4	67.3	56.9	19.8	9.3	17.2	17.1	36.5	47.4	34.9
Plain (P.S.)	44.5	67.6	56.9	25.6	3.7	3.2	25.4	29.6	50.0	34.1
Ribbed (P.S.)	43.4	66.3	57.9	25.7	2.8	3.3	20.7	35.1	46.0	33.5
Deviation (plain S.S. vs plain P.S.) %	5.0	0.5	0.0	28.8	-60.1	-81.5	49.0	-19.0	5.6	-2.4
Deviation (plain S.S. vs Ribbed P.S.) %	2.1	-1.4	1.7	29.7	-70.0	-80.8	21.5	4.0	-3.0	-4.1

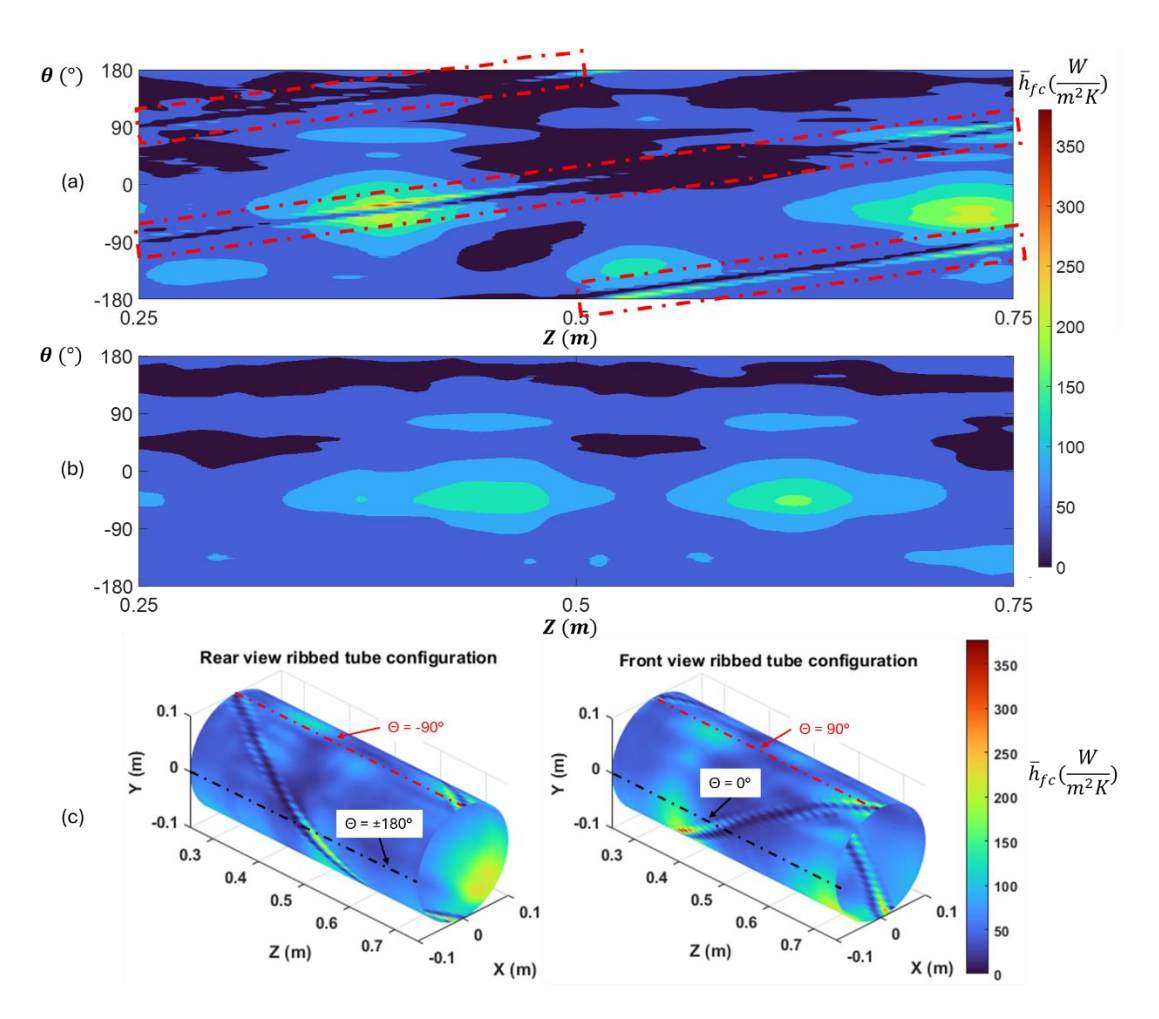


**Figure 6.** Average forced convection coefficient  $(\theta, Z)$  for the equivalent tube, averaged from 32 tubes in panel 2, for ribbed (a) (red dashed boxes shows corrugation position), plain (b) tubes receivers, and (c) cylindrical representation of ribbed tube configuration.

Receiver Finally, Figure 6 shows the local values of the air convection coefficient for an example panel with the largest convection coefficient (panel 2 according to Table 2), with the red dashed boxes indicating the location of the corrugations. The figure indicates that the peak and valley values of  $h_{fc}$  for the ribbed tube case (Figure 5(a)) are much lower and higher, respectively, than those for the plain tube (Figure 5(b)), which exhibits more uniform values along the tube. The highest peak in  $\bar{h}_{fc}{}_{panel\,j}(\theta)$  occurs with ribbing at  $\theta$  –40° and -95° and  $\bar{h}_{fc}{}_{panel\,j}(\theta)$  varies markedly with the corrugation position, which creates a flow perturbation and turbulence bursts anchoring repeated periodically along de Z-axis. Finally, Figure 6(c) has been included to provide additional clarity for the reader. It shows the distribution of  $\bar{h}_{fc}{}_{panel\,j}(\theta)$  for a ribbed tube, highlighting the main angular positions.

#### 5. Conclusions

The CFD simulations of the wind flow across a cylindrical tubular receiver, modelled in this work with tube resolution, reveals the following characteristics concerning the air convective losses in solar power tower receivers:

• The circumferential distribution of the wind convection coefficient,  $\bar{h}_{fc\_panel}(\theta)$ , over the absorber tubes of a common configuration of external central receiver is mostly non-symmetrical along  $\theta$  in the majority of the receiver panels. Edge effects and other factors (as wind detachment and channelling) can cause local values of h to significantly

exceed the average values predicted by the well-known Siebers & Kraabel correlation [1]. The average value for the receiver is in reasonable agreement with the Siebers & Kraabel correlation [1], with a deviation of -30.9%, which falls within the correlation uncertainty range of ±50% indicated in [1].

- The Simultaneous Simulation of the complete domain for plain tubes produced the most accurate results as it avoids piecewise iteration errors. The analysis revealed that panel 2 exhibits the largest convective coefficient, while panels 4, 5, 6, and 7 have lower values. The peak locations of  $\bar{h}_{fc\_panel}(\theta)$  along the tube circumference vary with the orientation,  $\beta$ , of the panel with regards wind direction.
- The results for the ribbed tubes receiver indicate that the ribbed configuration does not significantly affect the average forced convection coefficients compared to plain tubes. However, notable deviations of the local convection coefficient occur at some points due to corrugations. Ribbed tubes with ribbing at  $\theta$  –40° and -95° exhibited the highest  $\bar{h}_{fc,i,i}(\theta,Z)$ , doubling that of the plain tube, due to increased turbulence.
- An analysis performed with the plain tube showed that the Piecewise Simulation provides  $\bar{h}_{fc,i,j}(\theta,Z)$  results generally consistent with the Simultaneous Simulation, the more significant deviations being observed in panels 5 and 6.

# Data availability statement

Data supporting the findings of this study may be provided upon request.

#### **Author contributions**

José Martín-Martínez conceptualization, methodology, CFD simulations, validation, formal analysis, Investigation, writing – original draft, writing – review & editing. Rafael Pérez-Álvarez conceptualization, methodology, resources, writing – review & editing. Diego Martínez-Plaza Review & editing. Antonio Acosta-Iborra validation, supervision, writing – review & editing.

# **Competing interests**

The authors declare that they have no competing interests.

# **Funding**

The authors gratefully acknowledge the financial support provided by the Spanish Government under the grant PID2021-122895OB-I00 funded by MCIN / AEI / 10.13039 / 501100011033 and by "ERDF A way of making Europe".

#### References

- [1] D. L. Siebers and J. S. Kraabel, "Estimating convective energy losses from solar central receivers," United States: N. p., 1984. doi: https://doi.org/10.2172/6906848
- [2] M. R. Rodríguez-Sánchez, A. Soria-Verdugo, J. A. Almendros-Ibáñez, A. Acosta-Iborra, and D. Santana, "Thermal Design Guidelines of Solar Power Towers," Applied Thermal Engineering, vol. 63, no. 1, pp. 428–438, Jan. 2014, doi: <a href="https://doi.org/10.1016/j.ap-plthermaleng.2013.11.014">https://doi.org/10.1016/j.ap-plthermaleng.2013.11.014</a>
- [3] M. Cantone, M. Cagnoli, J. F. Reche, and L. Savoldi, "One-side heating test and modeling of tubular receivers equipped with turbulence promoters for solar tower applications," in Appl. Energy, vol. 277, 2020, pp. 115519, doi: <a href="https://doi.org/10.1016/j.apen-ergy.2020.115519">https://doi.org/10.1016/j.apen-ergy.2020.115519</a>

- [4] R. Pérez-Álvarez, A. Acosta-Iborra, and D. Santana, "Thermal and Mechanical Stresses in Bayonet Tubes of Solar Central Receivers Working with Molten Salt and Liquid Sodium," Results in Engineering, vol. 5, p. 100073, Jan. 2020, doi: https://doi.org/10.1016/j.rineng.2019.100073
- [5] J. Martin-Martinez and A. Acosta-Iborra, "Detailed numerical simulation of corrugated receiver tubes for molten salt solar power towers," Proc. of the XII Nat. and III Int. Conf. on Eng. Thermodynamics 12CNIT, June 29<sup>th</sup> July 1<sup>st</sup> 2022, Madrid, Spain, pp. 502-511.